Radio holographic filtering, error estimation, and quality control of radio occultation data

M. E. Gorbunov,[1] K. B. Lauritsen,[2] A. Rhodin,[3] M. Tomassini,[3] and L. Kornblueh[4]

Received 28 June 2005; revised 27 December 2005; accepted 13 February 2006; published 27 May 2006.

[1] Processing of radio occultation data requires filtering and quality control for the noise reduction and sorting out corrupted data samples. We introduce a radio holographic filtering algorithm based on the synthesis of canonical transform (CT2) and radio holographic focused synthesized aperture (RHFSA) methods. The field in the CT2-transformed space is divided by a reference signal to subtract the regular phase variation and to compress the spectrum. Next, it is convolved with a Gaussian filter window and multiplied by the reference signal to restore the phase variation. This algorithm is simple to implement, and it is numerically efficient. Numerical simulation of processing radio occultations with a realistic receiver noise indicates a good performance of the method. We introduce a new technique of the error estimation of retrieved bending angle profiles based on the width of the running spectra of the transformed wavefield multiplied with the reference signal. We describe a quality control method for the discrimination of corrupted samples in the L2 channel, which is most susceptible to signal tracking errors. We apply the quality control and error estimation techniques for the processing of data acquired by Challenging Minisatellite Payload (CHAMP) and perform a statistical comparison of CHAMP data with the analyses of the German Weather Service (DWD). The statistical analysis shows a good agreement between the CHAMP and DWD error estimates and the observed CHAMP–DWD differences. This corroborates the efficiency of the proposed quality control and error estimation techniques.

Citation: Gorbunov, M. E., K. B. Lauritsen, A. Rhodin, M. Tomassini, and L. Kornblueh (2006), Radio holographic filtering, error estimation, and quality control of radio occultation data, *J. Geophys. Res.*, *111*, D10105, doi:10.1029/2005JD006427.

1. Introduction

[2] Remote sensing of the Earth's atmosphere by radio occultations (RO) is a valuable source of information for weather prediction and climate monitoring [*Kursinski et al.*, 2000; *Hajj et al.*, 2002]. RO data contain information about atmospheric refraction (caused by real refractivity) and absorption (caused by imaginary refractivity). Refraction and absorption derived from microwave observations may allow the retrieval of humidity and temperature without additional information [*Kursinski et al.*, 2002; *Facheris and Cuccoli*, 2003; *Kirchengast and Høeg*, 2004; *Gorbunov and Kirchengast*, 2005a]. During the past 10 years a significant effort was put into solving the problem of deriving refraction and absorption. Intensive investigations during 2001–2004 resulted in the ultimate mathematical solution based on Fourier integral operators (FIO): canonical transform (CT) [*Gorbunov*, 2001, 2002a], full-spectrum inversion (FSI) [*Jensen et al.*, 2002, 2003], phase matching (PM) [*Jensen et al.*, 2004], and canonical transform of type 2 (CT2) [*Gorbunov and Lauritsen*, 2002, 2004b, 2004a]. The FSI and CT2 methods are most effective numerically. Both methods are implemented as a global FIO applied to the complete record of RO data, the FIO being a composition of a multiplication with a reference signal and a single global Fourier transform. As shown by *Pavelyev et al.* [2004], this reveals the relationship between the FIO-based methods, on one side, and the radio holographic (radio optics) methods of focused synthetic aperture (RHFSA) [*Igarashi et al.*, 2000; *Gorbunov et al.*, 2000; *Pavelyev et al.*, 2002].

[3] As any experimental data, RO measurements contain noise. The most important noise sources can be classified as follows: (1) instrumental noise, (2) ionospheric noise, and (3) noise due to small-scale turbulence. Ionospheric noise is the most significant error source for GPS occultations, while small-scale turbulence is expected to be the most important noise source for absorption retrieval from microwave occultations [*Gorbunov and Kirchengast*, 2005a]. One of the goals of this paper is the development of radio holographic filtering technique.

[4] Noise filtering has been used in all the existing algorithms for processing RO data, because the computation of bending angles requires the numerical differentiation of the phase retrieved from the experimental wavefield. Numerical simulations of CT and FSI inversion of RO data with additive white noise were performed by *Gorbunov et al.* [2004].

[1] Institute for Atmospheric Physics, Moscow, Russia.
[2] Danish Meteorological Institute, Copenhagen, Denmark.
[3] German Weather Service, Offenbach, Germany.
[4] Max-Planck Institute for Meteorology, Hamburg, Germany.

0148-0227/06/2005JD006427$09.00

[5] The RHFSA method using spectral analysis in sliding apertures can also be looked at as a filter applied to the complex field. A modification of this method using the CT analysis in sliding apertures (CTSS) was introduced by *Beyerle et al.* [2004]. Both RHFSA and CTSS approaches derive bending angles from the position of the maxima of the amplitude of the field transformed in each sliding aperture. *Gorbunov* [2002c] suggested combining the radio holographic analysis with back propagation. Another approach based on spectral weighting was introduced by *Sokolovskiy* [2001].

[6] *Lohmann et al.* [2003] suggested the use of Windowed FSI method (WFSI). *Lohmann et al.* [2006] reformulated WFSI in the frequency (approximately impact parameter) representation, similarly to *Gorbunov and Lauritsen* [2004c]. This method approximately computes each frequency component of the global Fourier transform by evaluating the Fourier integral in sliding windows centered at the stationary phase points for each frequency component. While, when using FSI, the noise in each frequency component originates from the complete time domain, in WFSI it only comes from the sliding window, which reduces the noise influence. The main drawback of this approach is its numerical inefficiency: because phase lapse rate significantly differs for different occultation fragments, the window width should be chosen different for different frequency components. Therefore WFSI filtering cannot be implemented as a convolution with a fixed window function, which makes this technique numerically inefficient.

[7] *Gorbunov and Lauritsen* [2004c] suggested a different approach to the filtering of RO data, which allows for an efficient numerical implementation. This approach employs the radio holographic principle [*Pavelyev et al.*, 2004], which is combined with the CT method. By the FIO, the wavefield is transformed into the impact parameter representation and divided by the reference signal. This operation removes the regular phase variation and compresses the spectrum. The signal with the compressed spectrum is convolved with a window function, and then it is multiplied by the reference signal to restore the original phase variation.

[8] Here we introduce a method of the estimation of the errors of the retrieved bending angles as a further development of the approach used by *Hocke et al.* [1999]. *Hocke et al.* [1999] estimated bending angle errors retrieved by the RHFSA method as full width of half maxima of the running spectra computed in the time domain. We use the radio holographic analysis of the transformed wavefield in the impact parameter domain, and estimate the bending angle error as the width of the running spectra of the transformed wavefield. Because in the impact parameter domain multipath is disentangled, this results in more accurate error estimate.

[9] Processing experimental RO data acquired by Challenging Minisatellite Payload (CHAMP), *Wickert et al.* [2001] poses an important problem of quality control (QC) to remove or suppress data samples corrupted to signal tracking errors. L2 channel is most susceptible to this type of errors, which typically occur under multipath condition. The development of QC procedure is the second goal of the paper.

[10] We introduce a QC procedure based on the radio holographic analysis of running spectra of the measured L1 and L2 wavefields in the time domain. Using the L2 spectral width and discrepancies between L1 and L2 spectral maxima we form an empirical penalty function discriminating corrupted data in the L2 channel.

[11] The estimation of observational errors and QC is necessary to optimally use RO data in atmospheric data assimilation. Data assimilation systems estimate the state of the atmosphere as a weighted mean of the previous forecast (which carries the information of observations earlier in time) and the observations at the current time, taking into account the errors of both the forecast and the observations. In order to get an optimal analysis, it is important to accurately estimate these error characteristics and to remove outliers from the data. The data assimilation scheme we are working on was discussed by *Gorbunov and Kornblueh* [2003]. We use a three-dimensional (3-D) forward modeling as the observational operator. The operator implements the computation of bending angles for a given observation geometry and 3-D atmospheric fields. Bending angles are computed from the modeled Doppler frequency shifts in exactly the same way as done in the processing of RO measurements. This observational operator is a physical model of RO observations with very few approximations. Its errors are defined by the model representation errors including the errors of the gridded atmospheric fields and the limited resolution. Bending angle as extracted from RO measurements is the observable. Therefore, for the standard data assimilation scheme we need to specify errors of observed and modeled bending angles. In this paper we present a technique for the estimation of the errors of the observed bending angles.

[12] *Healy et al.* [2005] demonstrated a positive forecast impact from CHAMP occultations even using some a priori fixed error estimates. For the optimal use of radio occultation data it is an advantage not to use static observational error estimates but to derive them from the actual data, because the accuracy of the retrieval strongly depends on the actual ionospheric activity, turbulence in the lower troposphere, and multipath conditions.

[13] The paper is organized as follows. In section 2 we describe the radio holographic filtering algorithm. In section 3 we discuss the error estimation. In section 4 we describe the QC algorithm of processing CHAMP data. In section 5 we present the numerical simulations of filtering noisy RO data and give examples of processing experimental data from CHAMP. The retrieved bending angle profiles and their errors are compared with corresponding profiles from the nearest 3-hourly forecasts of German Weather Service (Deutscher WetterDienst, DWD). Finally, we perform the statistical comparison of CHAMP bending angle and temperature profiles and their estimated errors with the respective profiles and error estimates of 3-hourly DWD analyses. These so-called innovation statistics are a common tool for the assessment of the consistency of the data and its information content for data assimilation purposes.

2. Radio Holographic Filtering

[14] Consider the wavefield $u(t) = A(t) \exp(ik\Psi(t))$ measured by LEO during a radio occultation experiment.

Measurements for each moment of time t may contain interfering wavefields from multiple interfering rays with different impact parameters p and bending angles ϵ. The separation of multiple rays and correction for diffraction effects due to big propagation distance from the planet limb is performed by a FIO (of the 2nd type) transforming the measured field into the representation of the impact parameter [*Gorbunov and Lauritsen*, 2002; *Jensen et al.*, 2004; *Gorbunov and Lauritsen*, 2004a, 2004b]:

$$\hat{\Phi}_2 u(p) = \sqrt{\frac{-ik}{2\pi}} \int a_2(p,t) \exp(ikS_2(p,t)) u(t)\, dt, \qquad (1)$$

where $a_2(p, t)$ is the amplitude function and $S_2(p, t)$ is the phase function. This operator separates the single ray with the given impact parameter p. Given the expression for the Doppler frequency $\eta = \dot{\Phi}$ as a function of the impact parameter p, GPS and LEO satellite radii $r_G(t)$, $r_L(t)$, and the satellite-to-satellite angle $\theta(t)$:

$$\eta(p,t) \equiv \dot{\theta} p + \frac{\dot{r}_L}{r_L}\sqrt{r_L^2 - p^2} + \frac{\dot{r}_G}{r_G}\sqrt{r_G^2 - p^2}, \qquad (2)$$

the phase function $S_2(p, t)$ equals $-\int \eta(p, t)dt$ [*Jensen et al.*, 2004; *Gorbunov and Lauritsen*, 2004a]. *Gorbunov and Lauritsen* [2004a] derived the accurate expression for the amplitude function $a_2(p, t)$ and constructed the approximation that generalizes the FSI method and reduces the FIO to a composition of the multiplication with a reference signal and a Fourier transform.

[15] Denote the field in the impact parameter representation $\hat{\Phi}_2 u(p) \equiv w(p) = A'(p) \exp(ik\Psi'(p))$. Bending angle $\epsilon(p)$ is an algebraic function of $d\Psi'(p)/dp$ [*Jensen et al.*, 2004; *Gorbunov and Lauritsen*, 2004a]. Under the assumption of spherical symmetry, amplitude $A'(p)$ is proportional to the integral absorption along the ray: $A'(p) = A'_0 \exp(-\tau(p)) = A'_0 \exp(-k\int N'' ds)$, where A'_0 is the normalizing constant, N'' is the imaginary refractivity, and $\tau(p)$ is transmission. Real and imaginary refractivity are derived from the bending and transmission by Abel transform [*Kursinski et al.*, 2002]. The general expression for $A'(p)$ and discussion of the absorption retrieval in presence of horizontal gradients by the differential method are given by *Gorbunov and Kirchengast* [2005a].

[16] The wavefield contains measurement noise. We apply the corresponding FIO to the noisy field without any prefiltering, because it was shown by *Gorbunov et al.* [2004] that CT/FSI techniques are robust with respect to noise. Consider the model of the phase variation $\Psi'_m(p)$ obtained by smoothing the phase $\Psi'(p)$ with a window of 0.25 km. The corresponding reference signal equals $w_m(p) = \exp(ik\Psi'_m(p))$. We define the radioholographic filter as follows:

$$\overline{w}(p) = w_m(p)\left(W(p) * \frac{w(p)}{w_m(p)}\right). \qquad (3)$$

Here $W(p)$ is the window function, which in this work is assumed to have the Gaussian form

$$W(p) = \frac{1}{\sqrt{2\pi}\sigma_p} \exp\left(-\frac{p^2}{2\sigma_p^2}\right), \qquad (4)$$

and σ_p is the filter width. The convolution in equation (3) allows a fast numerical implementation consisting of a fast Fourier transform (FFT) $F_{p\to\xi}$, multiplication with the Fourier-transformed window function, and the inverse FFT $F^{-1}_{\xi\to p}$:

$$\overline{w}(p) = w_m(p) F^{-1}_{\xi\to p}\left[F_{p\to\xi}[W] F_{p\to\xi}\left[\frac{w}{w_m}\right]\right]. \qquad (5)$$

3. Radio Holographic Error Estimation

[17] The error estimation of bending angles $\epsilon(p)$ in the lower troposphere is performed by the analysis of running spectra of the transformed wavefield $w(p)$. Radio holographic filtering is included into the data processing algorithm as an option, which can be turned on or off by the corresponding data processing script parameter. So the below consideration can be applied both to the unfiltered field $w(p)$ and filtered field $\overline{w}(p)$. The radio holographic filtering is effective for eliminating additive uncorrelated noise. The important errors source of CHAMP data in the lower troposphere is signal tracking errors in multipath areas, resulting in nonlinear signal distortions [*Ao et al.*, 2003; *Beyerle et al.*, 2003]. The radio holographic error estimation is aimed at accounting for the signal tracking errors.

[18] We utilize the phase variation model $\Psi'_m(p)$ and evaluate the running spectra:

$$w(p,\xi) = \int_{p-\Delta p}^{p+\Delta p} \frac{w(p')\left[1 + \cos\frac{\pi(p'-p)}{\Delta p}\right] \exp(-ik\xi p')}{2\exp\left(ik\Phi'_m(p')\right)} dp', \qquad (6)$$

where $\Delta p = 1.0$ km. The spectrum maximum is located on the average near $\xi = 0$. The tropospheric error of bending angle $\delta\varepsilon_T(p)$ is estimated as the spectral width:

$$\delta\varepsilon_T(p) = \left(\frac{\int |w(p,\xi)|^2 \xi^2 d\xi}{\int |w(p,\xi)|^2 d\xi}\right)^{1/2}. \qquad (7)$$

4. Quality Control of CHAMP Data

[19] The filtering and error estimation techniques described above are applied for the operational processing of CHAMP data. However, these techniques need to be complemented with a quality control (QC) procedure capable of dealing with signal tracking errors, which are a significant problem in the lower troposphere [*Gorbunov and Kornblueh*, 2003; *Beyerle et al.*, 2004]. The aim of the QC procedure is the removal of data samples corrupted due to signal tracking errors.

[20] At the first step, we make a rough estimation of bending angles in the geometric optical approximation (without any FIO-based processing), using a strong smoothing with a vertical scale of 2 km. The data where the estimated bending angle exceeds 0.02 rad are rejected, because the statistical analysis [*Gorbunov and Kornblueh*, 2003] indicates that such data are unusable.

[21] At the second step, we perform the analysis of running spectra $v_{1,2}(t, \eta)$ of L1 and L2 signals $u_{1,2}(t) = A_{1,2}(t) \exp[ik_{1,2}\Psi_{1,2}(t)]$:

$$v_{1,2}(t,\eta) = \int_{t-\Delta t}^{t+\Delta t} \frac{u_{1,2}(\tau)\left[1+\cos\frac{\pi(\tau-t)}{\Delta t}\right]\exp(-ik\eta\tau)}{2\exp\left[ik\left(\Phi_m(\tau)-\dot{\Phi}_m(t)\tau\right)\right]}d\tau, \quad (8)$$

where $\exp[ik\Psi_m(\tau)]$ is the reference signal, $\Psi_m(\tau)$ in each sliding aperture being a square polynomial obtained by regression from $\Psi(\tau)$ [*Gorbunov et al.*, 2000]. In each sliding aperture we remove the constant frequency $\dot{\Phi}_m(t)$ of the reference signal in the aperture center t.

[22] For the discrimination of L2 data with big noise level or lost signal tracking, we form the penalty function for L2 data describing the degradation of L2 data quality. For this purpose we estimate the average impact parameter and its spectral width:

$$\bar{p}_{1,2}(t) = \frac{\int |v_{1,2}(t,\eta)|^2 p(t,\eta)\, d\eta}{\int |v_{1,2}(t,\eta)|^2 \, d\eta}, \quad (9)$$

$$\delta p_{1,2}(t) = \left(\frac{\int |v_{1,2}(t,\eta)|^2 \left(p(t,\eta)-\bar{p}_{1,2}(t)\right)^2 d\eta}{\int |v_{1,2}(t,\eta)|^2 \, d\eta}\right)^{1/2}, \quad (10)$$

where $p(t, \eta)$ is the solution of equation (2) with respect to impact parameter p. The empirical penalty function is assumed to be equal to the following expression:

$$W(t) = 1 - \exp\left[-\frac{(\bar{p}_2(t)-\bar{p}_1(t))^2+\delta p_2^2(t)}{\Delta p^2}\right], \quad (11)$$

where Δp = 0.2 km. Increased spectral width $\delta p_2(t)$ and increased discrepancy between L1 and L2 average impact parameters $\bar{p}_2(t) - \bar{p}_1(t)$ characterize the degradation of the L2 data quality.

[23] From the running spectra we compute the smoothed phase paths: $\bar{\Phi}_{1,2}(t) = \int \bar{\eta}(t)dt$,where $\bar{\eta}(t)$ is the location of the maximum of the running spectrum at time t. The smoothed ionospheric difference of the optical paths is defined as $\Delta\bar{\Phi}(t) = \bar{\Phi}_2(t) - \bar{\Phi}_1(t)$ for the time interval where $W(t) < 0.7$. In the troposphere, where L2 data quality is typically very low, $\Delta\bar{\Phi}(t)$ is extrapolated. For this purpose we evaluate the linear regression of $\Delta\bar{\Phi}(t)$ between the time when the height of 30 km is reached and time when $W(t)$ reaches a value of 0.7. In the region where $W(t) > 0.7$ we define $\Delta\bar{\Phi}(t)$ as the extrapolation of the linear regression.

[24] Denote D_i the operation of taking finite differences of a gridded function: $D_iF = F(t_{i+1}) - F(t_i)$. Corrected phase path $\Psi_2^{\rm cor}(t)$ and amplitude $A_2^{\rm cor}(t)$ for the L2 channel are defined as a linear combination of L1 and L2 data with the weight defined by the penalty function $W(t)$:

$$D_i\Phi_2^{\rm cor} = D_i\Phi_2(1-W(t_i)) + (D_i\Phi_1 + D_i\Delta\bar{\Phi})W(t_i), \quad (12)$$

$$\Phi_2^{\rm cor}(t_i) = \sum_{j=1}^{i-1} D_j\Phi_2^{\rm cor}, \quad (13)$$

$$A_2^{\rm cor}(t_i) = A_1(t_i)(1-W(t_i)). \quad (14)$$

Note, CHAMP amplitude data for L2 channel, $A_2(t)$, contain high level of the instrumental noise, which makes them practically useless. So instead of original $A_2(t)$ we substitute $A_1(t)$. The finite differences are employed to get rid of arbitrary constants $\Psi_{1,2}^0$ in the definitions of L1 and L2 optical paths. The penalty function $W(t)$ is used to suppress the amplitude of corrupted L2 data to reduce their influence on the FIO-based processing algorithm.

[25] By the CT2 method, we compute L1 and L2 bending angles $\epsilon_{1,2}(p)$ from wavefields $u_1(t)$ and $u_2^{\rm cor}(t)$. The geometric optical shadow border p_1 is determined from the maximum of the correlation of $|\hat{\Phi}_2 u_1(p)|$ with a unit step function also referred to as θ function. For L2 data the maximum of the correlation of $|\hat{\Phi}_2 u_2(p)|$ with a θ function, p_2, defines the border below which L2 data are unusable. Because of the definition of $A_2^{\rm cor}(t)$, normally, $p_2 > p_1$, because corrupted L2 data are suppressed. For impact parameter interval $[p_1, p_2]$, L2 bending angles $\epsilon_2(p)$ are defined as $\epsilon_1(p) + \Delta\epsilon(p)$, where $\Delta\epsilon(p)$ is the estimate of the ionospheric difference $\epsilon_1(p) - \epsilon_2(p)$ computed over the impact parameter interval $[p_2, p_2 + 1$ km]. The ionospheric correction and the estimate of the residual ionospheric error $\delta\epsilon_I(p)$ of the neutral atmospheric bending angle profile $\epsilon(p)$ are described by *Gorbunov* [2002d].

[26] The RMS bending angle error $\delta\epsilon(p)$ is assumed to equal $\delta\epsilon_I(p) + \delta\epsilon_T(p)$, where $\delta\epsilon_T(p)$ is only estimated for ray height $p - r_E < 10$ km and it is neglected above 10 km. $\delta\epsilon_T(p)$ is only computed from the L1 error, because L2 data are suppressed by the penalty function in the areas where their error exceeds the L1 error. Some residual ionospheric correction error will arise due to L2 cutoff and the extrapolation of $\Delta\bar{\Phi}(t)$ below p_2 (S. Sokolovskiy, private communication, 2005). The RMS error of the Abel retrieval of $n(r)$ is estimated as follows:

$$\left\langle \delta n^2(x)\right\rangle = \frac{1}{\pi^2}\int_x^\infty\int \frac{\langle\delta\epsilon(p')\delta\epsilon(p'')\rangle dp'dp''}{\sqrt{p'^2-x^2}\sqrt{p''^2-x^2}}, \quad (15)$$

where the bending angle covariance $\langle\delta\epsilon(p')\delta\epsilon(p'')\rangle$ is equal to $\delta\epsilon^2(p)$ for $p' = p'' = p$, and elsewhere we assume the triangle covariance with a characteristic width of 1 km according to the estimations by *Vorob'ev and Kan* [1999].

[27] Under assumption that the correlation radius of δn is significantly smaller than the characteristic vertical scale of the atmosphere (about 7.5 km), the temperature retrieval error is approximately evaluated as follows:

$$\sigma_{\rm CHAMP} \equiv \left\langle \delta T^2\right\rangle^{1/2} = \left\langle \delta n^2\right\rangle^{1/2}\frac{T}{n-1}. \quad (16)$$

5. Results

[28] Figure 1 presents a numerical simulation of filtering noisy radio occultation data. We simulated an occultation at 10 GHz, using a simple spherically symmetrical refractivity field, including real and imaginary refractivity, $N(z)$ =

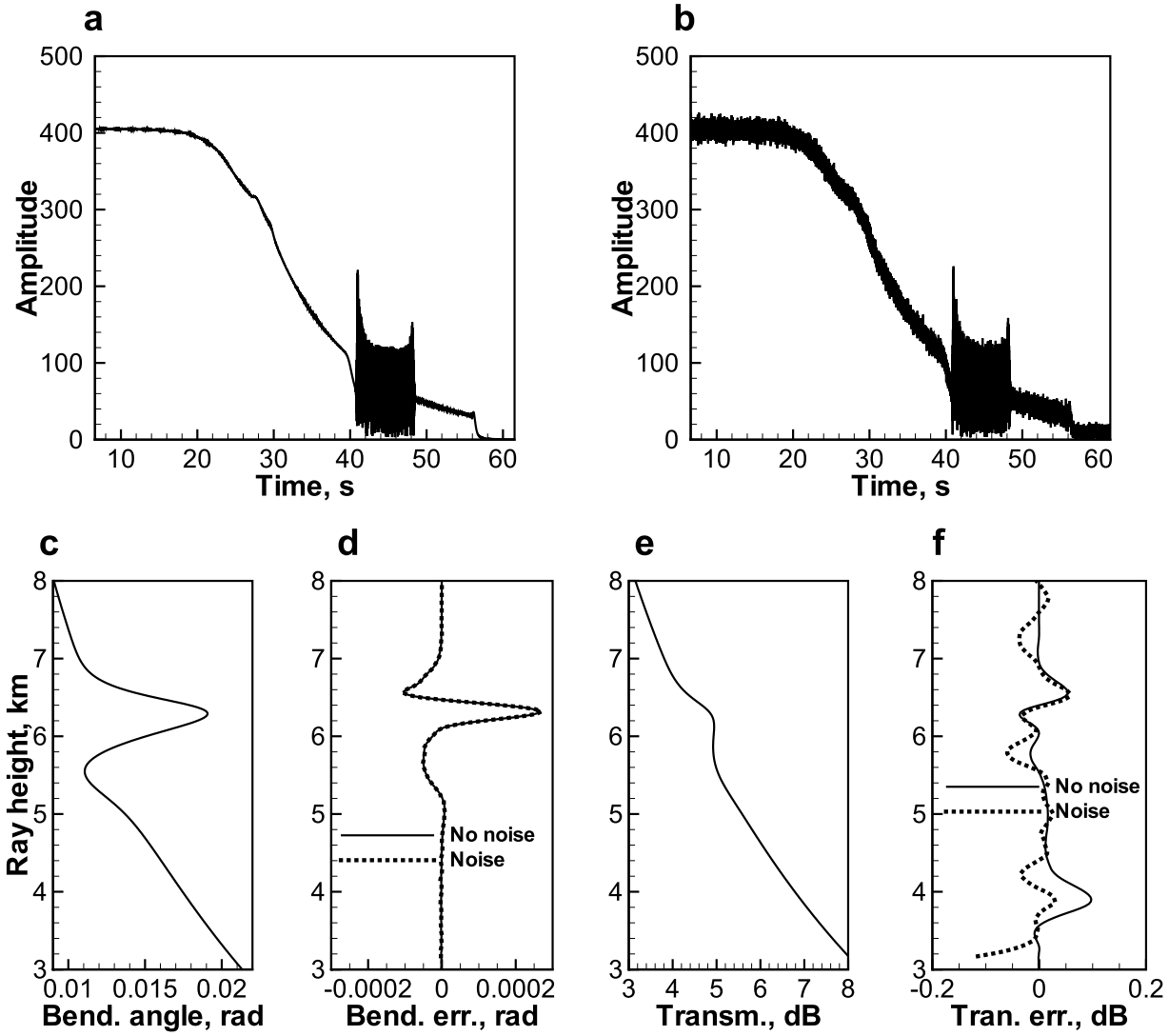

Figure 1. Processing simulated RO data with noise: (a) simulated amplitude without noise, (b) simulated amplitude with noise, (c) bending angle profile, (d) bending angle retrieval errors with and without noise, (e) transmission profile, and (f) transmission retrieval errors with and without noise.

$\mathrm{Re}[n(z)] - 1$ and $N''(z) = \mathrm{Im}[n(z)]$, respectively, similar to that used by *Lohmann et al.* [2003, 2006]:

$$N(z) = 315 \times 10^{-6} \exp\left(-\frac{z}{7.35\mathrm{km}}\right) + 20 \times 10^{-6} \cdot \exp\left(-\frac{(z-5\mathrm{km})^2}{(0.5\mathrm{km})^2}\right), \quad (17)$$

$$N''(z) = 3 \times 10^{-5} N(z). \quad (18)$$

We modeled a white additive receiver noise with a carrier-to-noise density of 60 dB Hz. This corresponds to a higher noise level compared to the assumed carrier-to-noise density of 67 dB Hz for the ACE+ Mission [*Kirchengast and Høeg*, 2004; *Gorbunov and Kirchengast*, 2005a]. Figure 1a presents the simulated amplitude without noise. The noisy amplitude is plotted in Figure 1b. Figure 1c presents the lower tropospheric bending angle profile. The bending angle errors with and without noise are plotted in Figure 1d. For the bending angle retrieval we used CT2 method with a radio holographic filter with a characteristic width σ_p = 250 m. Bending angle retrieval proves to be very stable with respect to the noise, because the results with and without noise are very close. Figure 1e shows the transmission in dB, (20/ln 10) $\tau(p)$. The retrieved transmission was additionally filtered with a characteristic window of 600 m. The transmission retrieval errors are presented in Figure 1f, which shows that the effect of the noise is more visible in transmission than in bending angles. However, the transmission retrieval errors are mostly below 0.05 dB and at some points they reach 0.1 dB.

[29] In order to illustrate the performance of the radio holographic error estimation technique, we simulated a realistic radio occultation. Forward simulation was based on 3-D fields of an analysis of European Centre for Medium Range Forecasts (ECMWF) with superimposed turbulence (modeling of turbulence is described by *Gorbunov and Kirchengast*

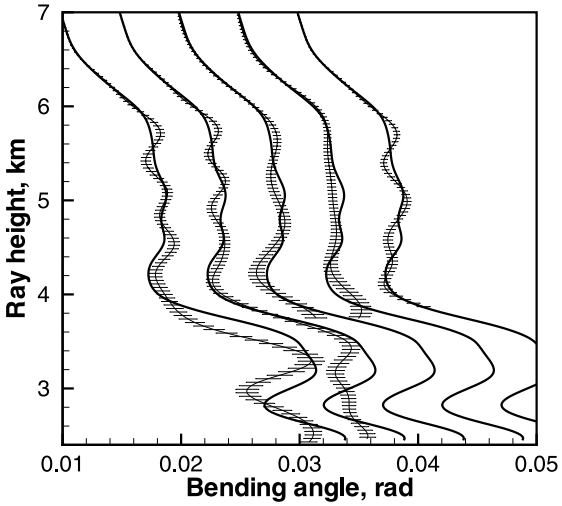

Figure 2. Simulation of signal tracking errors by a closed-loop receiver. Five realizations of random noise are shown with a horizontal shift of 0.005 rad. Heavy solid lines are the true bending angle profile; thin solid lines with error bars are retrieved bending angles with radio holographic error estimates.

[2005a, 2005b]). In the inversion we simulated signal tracking by a realistic closed-loop receiver model with a standard underdamped second-order loop with a bandwidth of 30 Hz [*Ao et al.*, 2003]. We also modeled a random receiver noise with a signal-to-carrier density of 45 dB Hz. Figure 2 presents five realizations of random noise, which are shown with a horizontal shift of 0.005 rad. Heavy solid lines are the true bending angle profile, thin solid lines with error bars are retrieved bending angles with radio holographic error estimates. Figure 2 shows that the radio holographic error estimates are close enough to the true errors.

[30] The filtering and error estimation techniques described above are applied for the operational processing of the RO data from CHAMP. Currently, CHAMP data are processed in real time using the computational facilities of Max-Planck Institute for Meteorology (Hamburg, Germany). Processing includes the standard geometric optical processing of stratospheric data above 15 km with a filter width of 1 km, the CT2 processing, radio holographic filtering with a filter width of 250 m, and radio holographic error estimation assuming a bending angle correlation radius of 1 km. The derived bending angles and temperatures are archived.

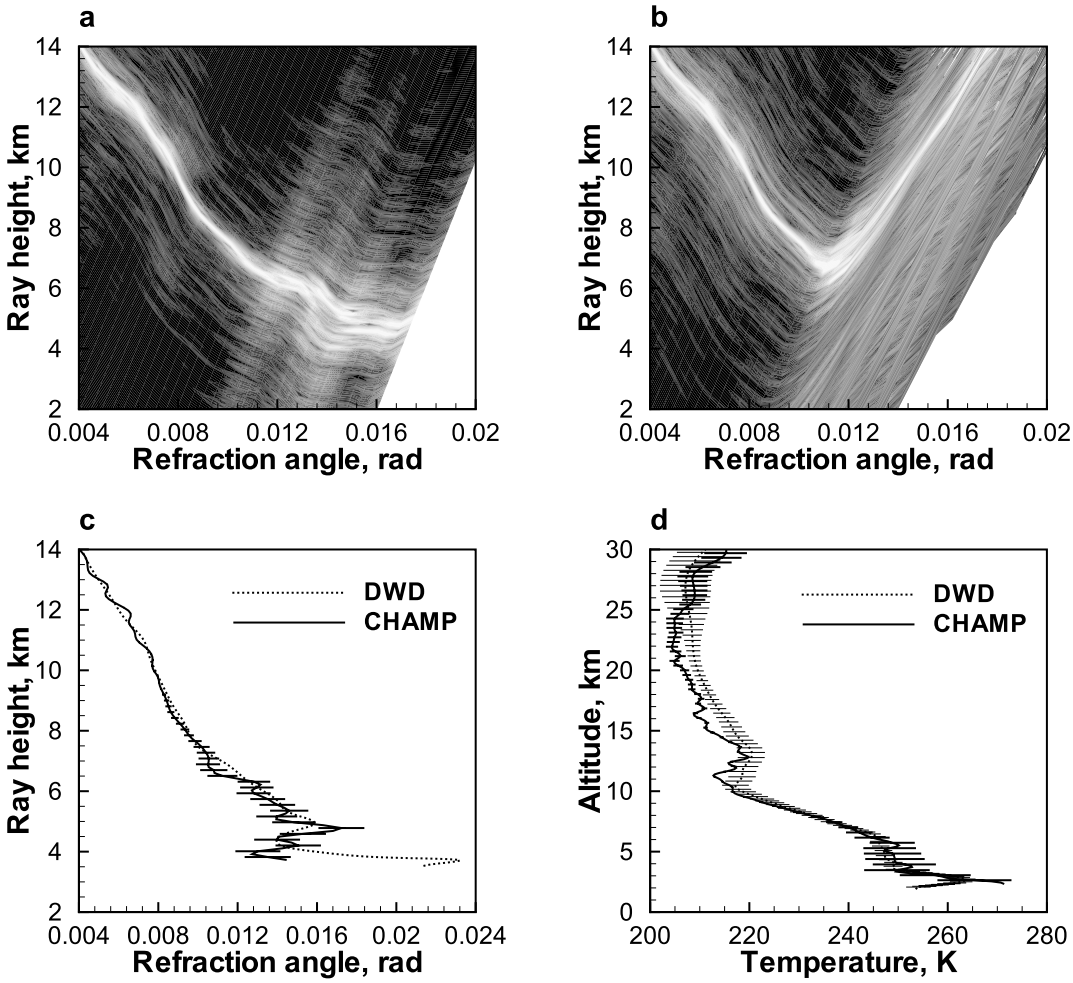

Figure 3. Occultation 0004, 18 January 2004, 0024 UTC, 50.4°N, 116.1°W: (a) L1 running spectra, (b) L2 running spectra, (c) bending angles: for DWD analysis and from CHAMP data, and (d) temperatures from DWD analysis and from CHAMP data.

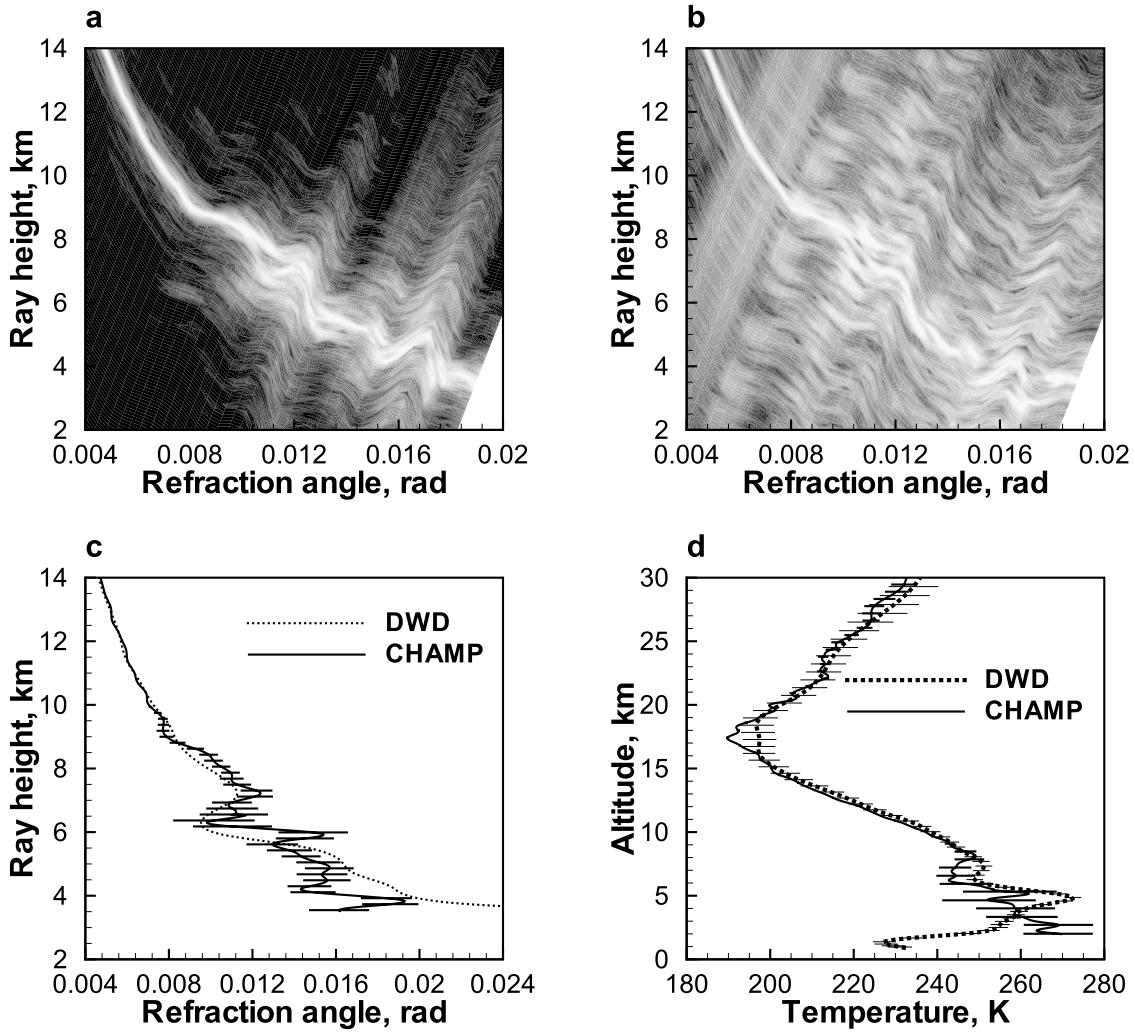

Figure 4. Occultation 0041, 18 January 2004, 0409 UTC, 26.0°S, 19.4°E: (a) L1 running spectra, (b) L2 running spectra, (c) bending angles for DWD analysis and from CHAMP data, and (d) temperatures from DWD analysis and from CHAMP data.

[31] Here we present the comparison of the bending angles and temperatures retrieved from CHAMP measurement with those computed from the nearest analysis of German Weather Service (Deutscher WetterDienst, DWD). It is important that the CHAMP–DWD difference includes both errors of CHAMP and DWD data. For the estimate of the degree of agreement between CHAMP and DWD data we also use the error estimate of the temperatures from the 3-hourly DWD forecasts σ_{DWD}. The horizontal grid of the DWD fields is an icosahedral grid with dimensions 128 × 128 × 10, which corresponds to a mesh size of about 55 km. The vertical grid has a resolution of 500–800 m below 10 km, and 900–2000 m between 10 and 20 km.

[32] Figure 3 presents an example of processing an occultation. Figures 3a and 3b show the running spectra $v(t, \eta)$ plotted in the ray coordinates: ray height $p - r_E$, where r_E is the Earth's radius, and bending angle ϵ [*Gorbunov*, 2002b]. For the L1 channel the bending angle profile is distinctly visualized for heights above 6.5 km. This fragment of the bending angle profiles is also well observed in the L2 spectra, although the L2 spectra are wider, which indicates lower quality of the L2 signal. Below 6.5 km, the L1 spectra have more complicated structure indicating the multipath propagation. In the L2 channel the situation is completely different. After the ray height reached 6.5 km, and bending angle reached 0.011 rad, both ray height and bending angle begins to rapidly increase. This indicates that in the L2 channel the signal track was lost. Figures 3c and 3d show the retrieved bending angles and dry temperatures, compared with DWD bending angles and dry temperatures. Also plotted are the error estimates for CHAMP bending angles and for both CHAMP and DWD dry temperatures. The DWD temperature and bending angle profiles are computed from the 3-hourly forecast as used in the operational data assimilation system. The temperature errors are derived from statistics of observations minus first guess, taking into account the accuracy of the previous analysis. There are indications that these estimates are too large and currently the DWD forecast error estimates are being revised.

[33] Above 25 km the temperature retrieval errors due to background ionospheric scintillations, increase and reach

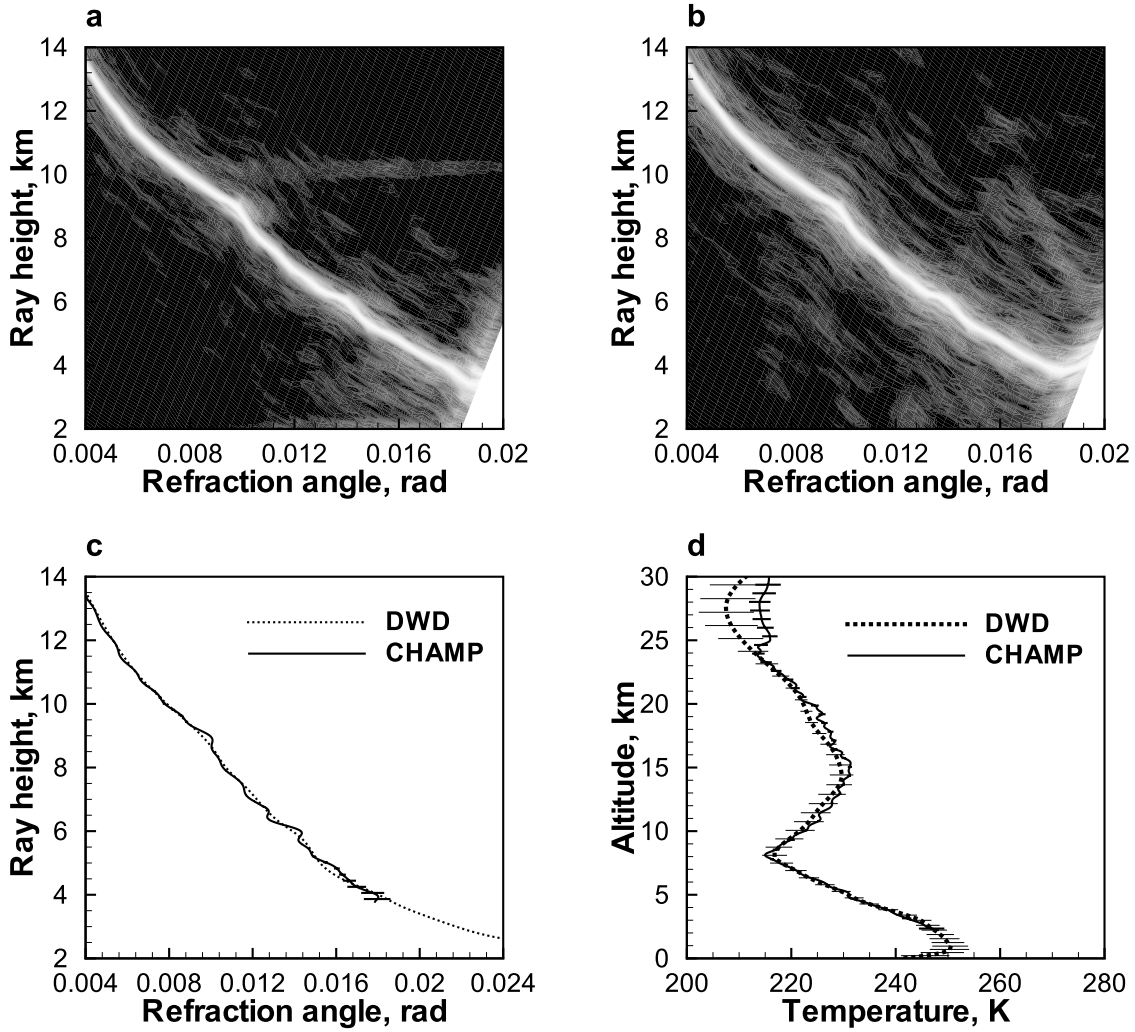

Figure 5. Occultation 0097, 18 January 2004, 0950 UTC, 78.8°N, 125.6°W: (a) L1 running spectra, (b) L2 running spectra, (c) bending angles: for DWD analysis and from CHAMP data, and (d) temperatures from DWD analysis and from CHAMP data.

5 K at 30 km. Between 25 and 7 km the temperature error estimates are below 1 K, because in this height interval bending angles are big enough compared to background ionospheric scintillations, and multipath propagation effects are insignificant for GPS frequencies. Below 7 km, multipath propagation manifests itself in nonmonotonous bending angle profiles both for CHAMP and DWD data and in the increase of error estimates for the CHAMP data.

[34] Figure 4 exemplifies the processing of another occultation. Here the ionospheric fluctuation is weaker than in the previous example, and the estimate of the temperature retrieval error is about 3 K at 30 km. Below 8 km the bending angle profile is nonmonotonous, which indicates multipath propagation. The spectra show strong noise in the L2 channel below 12 km. In the multipath areas the L2 noise significantly increase. Because of multipath, the temperature retrieval error below 7 km reaches 5–10 K. Figure 5 gives an example of an occultation with a good signal quality and low errors. In all the above examples, the discrepancy between CHAMP and DWD data agrees well with the error estimates and does not exceed $2(\sigma^2_{\mathrm{CHAMP}} + \sigma^2_{\mathrm{DWD}})^{1/2}$.

[35] Figure 6 (left) presents the statistical comparison of the CHAMP and DWD temperatures on the material of 90 occultations observed during 18 January 2004. We use the comparison technique based on the 3-D forward modeling as described by *Gorbunov and Kornblueh* [2003]. This approach excludes the comparison errors due to the horizontal gradients. The systematic CHAMP–DWD difference does not exceed 0.5 K above 5 km. The RMS deviation is 2–4 K. As shown by *Gorbunov and Kornblueh* [2001, 2003], below 5 km the systematic difference can reach 4 K. Here we only give the statistical comparison above 3 km, where the systematic difference does not exceed 1 K. The increase of the systematic errors in the lower troposphere results from the unstable operation of the receiver in multipath areas. This comparison is similar to those presented by *Kuo et al.* [2004], *Hajj et al.* [2004], and *Steiner and Kirchengast* [2005]. Figure 6 (right) shows the comparison of the RMS CHAMP–DWD difference with the

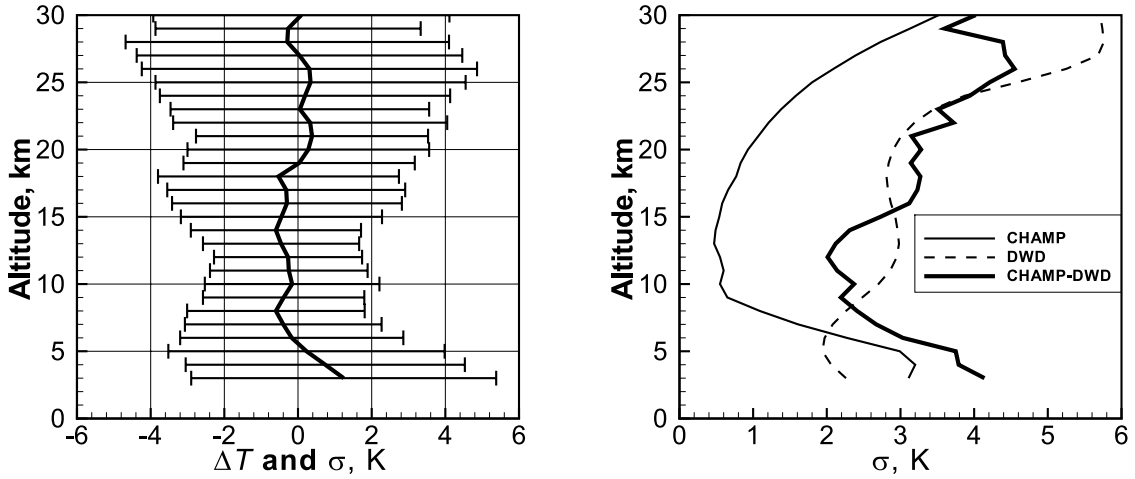

Figure 6. (left) Statistical comparison of temperatures retrieved from CHAMP data with DWD forecasts, 18 January 2004, bias and RMS deviation. (right) Estimated RMS errors of CHAMP temperature retrievals and DWD forecasts and actual innovations (retrieval minus forecast differences).

error estimates of the CHAMP and DWD data, σ_{CHAMP} and σ_{DWD}, respectively. The errors are averaged over the 90 occultation. Figure 6 indicates a reasonable agreement between the CHAMP and DWD error estimates, on one side, and the CHAMP−DWD difference, on the other side. In the height interval 8−15 km and above 24 km we notice the overestimation of the DWD errors.

6. Conclusions

[36] Using the radio holographic principle in combination with FIO-based data processing techniques, we introduced filtering, error estimation, and quality control algorithms. The radio holographic filtering of additive noise is applied to the transformed wavefield in the impact parameter domain. The spectrum of the signal is compressed by dividing the field by a reference signal, the signal is convolved with a fixed-width window function, and multiplied with the reference signal. This algorithm is simple and numerically efficient, its performance was corroborated by a numerical simulation of processing RO data with a realistic level of receiver noise. The noise filtering algorithm can be useful for the retrieval of absorption from microwave RO data. The error estimation of retrieved bending angles uses the radio holographic analysis of the transformed wavefield. The bending angle errors are estimated as the widths of running spectra. This error estimation does not require any a priori information. Processing experimental data requires the quality control in order to discriminate data samples corrupted due to signal tracking losses. Our QC procedure forms the penalty function, which is computed by the radioholographic analysis of L1 and L2 fields in the time domain. The criteria for the discrimination of corrupted L2 data samples include large spectral width corresponding to multipath propagation and large discrepancies between L1 and L2 spectral maxima characteristic for signal tracking loss. The comparison of the individual and statistically averaged error estimates of CHAMP data and DWD analyses for one day of observations, on one side, and the CHAMP−DWD deviation, shows that the error estimates and the deviations are consistent. The fact that the estimated observational errors are generally lower than the forecast errors indicates that the data contain considerable amount of information useful for data assimilation purposes. Using these error estimation and quality control techniques we developed robust algorithms, which are currently employed for the operational processing of CHAMP data at Max-Planck Institute for Meteorology and German Weather Service.

[37] **Acknowledgment.** This work was performed with the financial support of Max-Planck Institute for Meteorology (Hamburg, Germany), German Weather Service (Offenbach, Germany), Danish Meteorological Institute (Copenhagen), EUMETSAT (GRAS Meteorology SAF, DMI), and Russian Foundation for Basic Research (grant 03-05-64366). We are grateful to G. Beyerle for valuable consultations on receiver modeling.

References

Ao, C. O., T. K. Meehan, G. A. Hajj, A. J. Mannucci, and G. Beyerle (2003), Lower troposphere refractivity bias in GPS occultation retrievals, *J. Geophys. Res.*, *108*(D18), 4577, doi:10.1029/2002JD003216.

Beyerle, G., M. E. Gorbunov, and C. O. Ao (2003), Simulation studies of GPS radio occultation measurements, *Radio Sci.*, *38*(5), 1084, doi:10.1029/2002RS002800.

Beyerle, G., J. Wickert, T. Schmidt, and C. Reigber (2004), Atmospheric sounding by global navigation satellite system radio occultation: An analysis of the negative refractivity bias using CHAMP observations, *J. Geophys. Res.*, *109*, D01106, doi:10.1029/2003JD003922.

Facheris, L., and F. Cuccoli (2003), Analysis of differential spectral attenuation measurements applied to a LEO-LEO link, ESA-ACEPASS Report (contract 16743/02/NL/FF), Inst. of Elect. and Telecommun., Univ. of Florence, Florence, Italy.

Gorbunov, M. E. (2001), Radioholographic methods for processing radio occultation data in multipath regions., *Sci. Rep. 01-02*, Dan. Meteorol. Inst., Copenhagen. (Available at http://web.dmi.dk/dmi/Sr01-02.pdf)

Gorbunov, M. E. (2002a), Canonical transform method for processing radio occultation data in the lower troposphere, *Radio Sci.*, *37*(5), 1076, doi:10.1029/2000RS002592.

Gorbunov, M. E. (2002b), Radio-holographic analysis of Microlab-1 radio occultation data in the lower troposphere, *J. Geophys. Res.*, *107*(D12), 4156, doi:10.1029/2001JD000889.

Gorbunov, M. E. (2002c), Radioholographic analysis of radio occultation data in multipath zones, *Radio Sci.*, *37*(1), 1014, doi:10.1029/2000RS002577.

Gorbunov, M. E. (2002d), Ionospheric correction and statistical optimization of radio occultation data, *Radio Sci.*, *37*(5), 1084, doi:10.1029/2000RS002370.

Gorbunov, M. E., and G. Kirchengast (2005a), Advanced wave-optics processing of LEO-LEO radio occultation data in presence of turbulence, *Tech. Rep. ESA/ESTEC 1/2005*, Univ. of Graz, Graz, Austria.

Gorbunov, M. E., and G. Kirchengast (2005b), Processing X/K band radio occultation data in the presence of turbulence, *Radio Sci.*, *40*, RS6001, doi:10.1029/2005RS003263.

Gorbunov, M. E., and L. Kornblueh (2001), Analysis and validation of GPS/MET radio occultation data, *J. Geophys. Res.*, *106*, 17,161–17,170.

Gorbunov, M. E., and L. Kornblueh (2003), Analysis and validation of Challenging Minisatellite Payload (CHAMP) radio occultation data, *J. Geophys. Res.*, *108*(D18), 4584, doi:10.1029/2002JD003175.

Gorbunov, M. E., and K. B. Lauritsen (2002), Canonical transform methods for radio occultation data, *Sci. Rep. 02–10*, Dan. Meteorol. Inst., Copenhagen. (Available at http://www.dmi.dk/dmi/Sr02-10.pdf)

Gorbunov, M. E., and K. B. Lauritsen (2004a), Analysis of wave fields by Fourier integral operators and their application for radio occultations, *Radio Sci.*, *39*, RS4010, doi:10.1029/2003RS002971.

Gorbunov, M. E., and K. B. Lauritsen (2004b), Canonical transform methods for radio occultation data, in *Occultations for Probing Atmosphere and Climate*, edited by G. Kirchengast, U. Foelsche, and A. K. Steiner, pp. 61–68, Springer, New York.

Gorbunov, M. E., and K. B. Lauritsen (2004c), Radio holographic filtering of noisy radio occultations, in *OPAC-2 Conference*, Inst. for Geophys., Astrophys., and Meteorol., Graz, Austria.

Gorbunov, M. E., A. S. Gurvich, and L. Kornblueh (2000), Comparative analysis of radioholographic methods of processing radio occultation data, *Radio Sci.*, *35*, 1025–1034.

Gorbunov, M. E., H.-H. Benzon, A. S. Jensen, M. S. Lohmann, and A. S. Nielsen (2004), Comparative analysis of radio occultation processing approaches based on Fourier integral operators, *Radio Sci.*, *39*, RS6004, doi:10.1029/2003RS002916.

Hajj, G. A., E. R. Kursinski, L. J. Romans, W. I. Bertinger, and S. S. Leroy (2002), A technical description of atmospheric sounding by gps occultation, *J. Atmos. Sol. Terr. Phys.*, *64*, 451–469.

Hajj, G. A., C. O. Ao, B. A. Iijima, D. Kuang, E. R. Kursinski, A. J. Mannucci, T. K. Meehan, L. J. Romans, M. de la Torre Juarez, and T. P. Yunck (2004), CHAMP and SAC-C atmospheric occultation results and intercomparisons, *J. Geophys. Res.*, *109*, D06109, doi:10.1029/2003JD003909.

Healy, S. B., A. M. Jupp, and C. Marquardt (2005), Forecast impact experiment with GPS radio occultation measurements, *Geophys. Res. Lett.*, *32*, L03804, doi:10.1029/2004GL020806.

Hocke, K., A. G. Pavelyev, O. I. Yakovlev, L. Barthes, and N. Jakowski (1999), Radio occultation data analysis by the radioholographic method, *J. Atmos. Sol. Terr. Phys.*, *61*, 1169–1177.

Igarashi, K., A. Pavelyev, K. Hocke, D. Pavelyev, I. A. Kucherjavenkov, S. Matyugov, A. Zakharov, and O. Yakovlev (2000), Radio holographic principle for observing natural processes in the atmosphere and retrieving meteorological parameters from radio occultation data, *Earth Planets Space*, *52*, 893–899.

Jensen, A. S., H.-H. Benzon, and M. S. Lohmann (2002), A new high resolution method for processing radio occultation data, *Sci. Rep. 02–06*, Dan. Meteorol. Inst., Copenhagen.

Jensen, A. S., M. S. Lohmann, H. Benzon, and A. S. Nielsen (2003), Full Spectrum Inversion of radio occultation signals, *Radio Sci.*, *38*(3), 1040, doi:10.1029/2002RS002763.

Jensen, A. S., M. S. Lohmann, A. S. Nielsen, and H. Benzon (2004), Geometrical optics phase matching of radio occultation signals, *Radio Sci.*, *39*, RS3009, doi:10.1029/2003RS002899.

Kirchengast, G., and P. Høeg (2004), The ACE+ mission: Atmosphere and climate explorer based on GNSS-LEO and LEO-LEO radio occultation, in *Occultations for Probing Atmosphere and Climate*, edited by A. K. S. G. Kirchengast and U. Foelsche, pp. 201–220, Springer, New York.

Kuo, Y.-H., T.-K. Wee, S. Sokolovskiy, C. Rocken, W. Schreiner, D. Hunt, and R. A. Anthes (2004), Inversion and error estimation of GPS radio occultation data, *J. Meteorol. Soc. Jpn.*, *82*, 507–531.

Kursinski, E. R., G. A. Hajj, S. S. Leroy, and B. Herman (2000), The GPS radio occultation technique, *Terr. Atmos. Oceanic Sci.*, *11*, 53–114.

Kursinski, E. R., S. Syndergaard, D. Flittner, D. Feng, G. Hajj, B. Herman, D. Ward, and T. Yunck (2002), A microwave occultation observing system optimized to characterize atmospheric water, temperature and geopotential via absorption, *J. Atmos. Oceanic Technol.*, *19*, 1897–1914.

Lohmann, M. S., A. S. Jensen, H.-H. Benzon, and A. S. Nielsen (2003), Radio occultation retrieval of atmospheric absorption based on F SI, *Sci. Rep. 03–20*, Dan. Meteorol. Inst., Copenhagen.

Lohmann, M. S., A. S. Jensen, H.-H. Benzon, and A. S. Nielsen (2006), Application of window functions for Full Spectrum Inversion of LEO-LEO radio occultation data, *Radio Sci.*, doi:10.1029/2005RS003273, in press.

Pavelyev, A., K. Igarashi, C. Reigber, K. Hocke, J. Wickert, G. Beyerle, S. Matyugov, A. Kucherjavenkov, D. Pavelyev, and O. Yakovlev (2002), First application of the radioholographic method to wave observations in the upper atmosphere, *Radio Sci.*, *37*(3), 1043, doi:10.1029/2000RS002501.

Pavelyev, A. G., Y. A. Liou, and J. Wickert (2004), Diffractive vector and scalar integrals for bistatic radio holographic remote sensing, *Radio Sci.*, *39*, RS4011, doi:10.1029/2003RS002935.

Sokolovskiy, S. V. (2001), Modeling and inverting radio occultation signals in the moist troposphere, *Radio Sci.*, *36*, 441–458.

Steiner, A. K., and G. Kirchengast (2005), Error analysis for GNSS radio occultation data based on ensembles of profiles from end-to-end simulations, *J. Geophys. Res.*, *110*, D15307, doi:10.1029/2004JD005251.

Vorob'ev, V. V., and V. Kan (1999), Background fluctuations measured by the radio sounding of the ionosphere in the GPS-Microlab-1 experiment, *Izv. Vissh. Ucheb. Zavedeniy Radiofiz.*, *XLII*, 511–523.

Wickert, J., et al. (2001), Atmosphere sounding by GPS radio occultation: First results from CHAMP, *Geophys. Res. Lett.*, *28*(17), 3263–3266.

M. E. Gorbunov, Institute for Atmospheric Physics, Pyzhevsky per. 3, Moscow 119017, Russia. (gorbunov@dkrz.de)

L. Kornblueh, Max-Planck Institute for Meteorology, Hamburg, Germany.

K. B. Lauritsen, Danish Meteorological Institute, Lyngbyvej 100, Copenhagen DK-2100, Denmark.

A. Rhodin and M. Tomassini, German Weather Service, Offenbach, Germany.